Random speckle patterns with azimuthal propagation order

Pau Riera Rodriguez* **and Rafael Piestun**

Department of Electrical, Computer, and Energy Engineering, University of Colorado Boulder, Boulder, CO 80309, USA

*pau.rierarodriguez@colorado.edu

Abstract: Speckle patterns stem from the interference of highly coherent waves having random phases and amplitudes. They are a significant limitation in imaging, including optical coherence tomography, radar, and ultrasound. Remarkably, they are also of fundamental interest for intentional applications in microscopy, metrology, optical computing, and light-matter manipulations. Furthermore, the synthesis of tailored speckle patterns is promising to optimize the performance of modern imaging and sensing systems. Here, we investigate the possibility of generating random speckle patterns with propagation order, namely 3D light fields whose transverse intensity distributions present speckle patterns that, despite being random at any location, present ordered non-random characteristics as a three-dimensional (3D) wave. In particular, we explore speckle propagation invariance through a superposition of Laguerre-Gaussian (LG) modes with arbitrary complex coefficients. By carefully applying constraints in the LG modal plane, we gain control over the behavior of speckles during propagation, enabling the repetition and rotation of the intensity speckle distribution while maintaining a random process across transverse planes. As a result, we introduce a degree of order in stochastic speckle patterns normally associated with non-random waves. The order–disorder coexistence is explained by the random superposition of modes, albeit conveying information in the phase of the field that preserves a delicate balance among wavefront dislocations with angular momentum and the Gouy phase shift of the corresponding modes. The experiments demonstrate speckle patterns with azimuthal propagation invariance and a framework for understanding, analyzing, and synthesizing stochastic speckle patterns with propagation-invariant properties.

1. Introduction

Speckle patterns are complex spatial fields arising from the interference of random coherent fields having a granular, random intensity distribution [1,2]. They are commonly generated when a coherent light source is reflected from a rough surface, transmitted through a diffuser, propagated along a multimode waveguide, or tailored by a Spatial Light Modulator (SLM) [3-11]. The resultant space-dependent constructive and destructive interference gives rise to bright and dark spots, respectively. Since the granular appearance of speckles is stochastic, they are typically described by their statistical properties. In the case of fully developed speckle patterns, the intensity distribution follows a negative exponential Probability Density Function (PDF) while the modulo of the amplitude follows Rayleigh statistics [2].

Recent work has demonstrated the possibility of tailoring speckle statistics in three dimensions and spectrally [3-11]. Because speckle wave-fields are a particular class of the whole class of solutions of the wave equation, they are naturally amenable to analysis via traditional wave-propagation methods and to synthesis via holographic and diffractive optics techniques [12-14]. As a result, if a particular speckle field is a feasible solution of the appropriate (4D space-time) wave equation, it is possible to synthesize it [12-14]. Accordingly, several methods have emphasized customization of speckles to obey specific statistical properties during propagation [3-

11]. Other solutions to non-diffracting speckle patterns have recently been proposed [15-17]. Therefore, the ability to control speckle properties is intriguing and can play a critical role in different scientific and technological areas such as dynamic speckle illumination [18,19], super-resolution microscopy [20-28], optical manipulation [29-31], computational ghost imaging [32-34] or customization of optical potentials [35,36].

In this work, we investigate the engineering of speckle patterns exhibiting order-disorder coexistence through the propagation invariance characteristics. The generating waves are exact solutions of the wave equation and thus define the whole class of propagation-invariant speckle fields. Different modal sets are possible, including Hermite-Gaussian, Laguerre-Gaussian, Ince-Gaussian, or Bessel beams. Here we present the analysis based on LG beams. We start by superimposing a balanced number of LG modes with specific modal distributions and randomized complex coefficients. This leads to random speckle patterns with transverse intensity repetition through propagation, a phenomenon known as the scaled self-imaging effect [37,38]. Furthermore, one generalization of this phenomenon is the rotating or azimuthal self-imaging effect [38], whereas the intensity distribution of the light beam appears rotated at specific spatial locations [38,39]. As a result, it is possible to maintain a degree of order in complex disordered fields. This approach demonstrates that complex fields can be engineered for applications requiring simultaneously randomness and structured propagation while preserving Orbital Angular Momentum (OAM) [40]. We further characterize the statistical properties of the speckle patterns of exemplary waves, demonstrating super-Rayleigh behavior. Finally, we experimentally generate phase-only computer-generated holograms on an SLM to validate the key properties. For simplicity, we refer to these fields as scaled self-imaging speckles (SSIS) and azimuthal self-imaging speckles (ASIS). Figure 1 represents schematically the class of speckle patterns with azimuthal order, showcasing rotating correlated speckles through propagation with the corresponding Normalized Cross-Correlation (NCC) at different transverse planes.

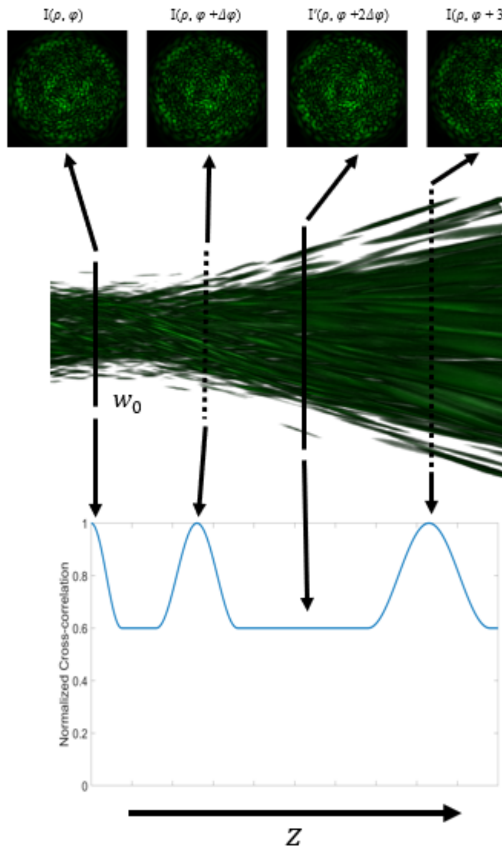

Figure 1. **Engineered speckle patterns with propagation order:** The intensity at four transverse planes is represented with the corresponding normalized cross-correlation at the bottom, indicating the occurrence of high correlation states with the intensity plane at w_0 through propagation. The dashed lines represent locations of intensity reoccurrences with possible rotation of the speckle pattern at different transverse crossections. The first solid line indicates the reference beam waist and the second solid line indicates a plane with no significant correlation with the intensity in the beam waist.

2. Theory

The Talbot effect [41] establishes that transverse fields with a periodic structure reveal replication of intensity patterns through propagation in the paraxial regime. Montgomery established the periodic repetition of the transverse intensity distribution of more general wave fields [42]. A generalization of this periodicity includes wave-fields exhibiting azimuthal rotations through propagation, including non-periodic fields [38,39]. We follow this latter formalism in the paraxial regime but, through the implementation of random coefficients, seek speckled scalar wave fields governed by the paraxial wave equation described as

$$\nabla^2 U + 2ik^2 \frac{\partial U}{\partial z} + 2k^2 U = 0 \tag{1}$$

where $k = \frac{2\pi}{\lambda}$ is the wave number, ∇^2 the transverse Laplace operator, and $U(\boldsymbol{r})$ is the complex field amplitude in cylindrical coordinates, $\mathbf{r} = (\rho,\ \varphi,\ z)$. This can be further expressed as a superposition of LG modes of the form

$$LG_p^l(\rho,\ \varphi,\ z) = C\frac{1}{\omega(z)}\left(\frac{r\sqrt{2}}{\omega(z)}\right)^{|l|}\exp\left(-\frac{r^2}{\omega^2(z)}\right)\ L_p^{|l|}\left(\frac{2r^2}{\omega^2(z)}\right)\times$$
$$\exp\left(-ik\frac{r^2}{2R(z)}\right)\ \exp\left(-\frac{r^2}{\omega^2(z)}\right)\exp(-il\phi)\ \exp(-i\psi(z)) \quad (2)$$

where z is the axial distance from the beam waist, $\omega(z)$ is the Gaussian spot size at position z, R is the radius of curvature, C is a normalization constant, p is the radial index, $|l|$ is the azimuthal index representing the topological charge, $L_p^{|l|}$ is the associated Laguerre polynomial, and $\psi(z) = \arctan\left(\frac{z}{z_R}\right)$ is the Gouy phase, where $z_R = \frac{\pi\omega_0^2}{\lambda}$, the Rayleigh range. The random speckle field amplitude can be decomposed into a superposition of LG beams that defines the complex amplitude as a linear combination of LG modes:

$$U(\rho,\ \varphi,\ z) = \sum_{p,l} c_{p,l} LG_p^l(\rho,\ \varphi,\ z) \quad (3)$$

where $c_{p,l}$ indicated the randomly selected coefficient intrinsic of each mode $LG_p^l(\rho,\ \varphi,\ z)$. By carefully selecting and applying a set of constraints in the LG modal plane, one can gain control over the behavior of the wave field through propagation. We focus on two constraints that lead to propagation invariance, which include selecting modes along parallel equidistant lines in the modal plane, as shown in Figure 2 [38].

In the first case study, the modes are aligned along horizontal straight lines (Fig. 2.a) such that self-images satisfy the following relation:

$$|U(\rho,\ \varphi,\ z+\ \Delta z)|^2 =\ |\mathcal{S}[\alpha]U(\rho,\ \varphi,\ z)|^2 \quad (4)$$

where Δz is the recurrence distance, which is dependent on the modal spacing, the scaling operator is defined as $\mathcal{S}[\alpha]U(x,y) = \alpha^2 U(\alpha x, \alpha y)$, and $\alpha = \frac{\omega(z)}{\omega(z+\ \Delta z)}$. Eq. (4) indicates that the intensity pattern is replicated at a different position along the z-axis. The phases are similarly scaled up to the addition of a quadratic phase [38].

In the second case study, the modes are aligned along inclined straight lines (Fig. 2.b) such that speckle patterns at different transverse planes appear rotated azimuthally. The complex amplitude follows the following relation:

$$|U(\rho,\ \varphi,\ z+\ \Delta z)|^2 =\ |\mathcal{S}[\alpha]U(\rho,\ \varphi+\ \Delta\varphi,\ z)|^2 \quad (5)$$

where $\Delta\varphi$ represents the angular rotation after propagation Δz. The phases are similarly scaled and rotated up to the addition of a quadratic phase [38]. When these constraints are applied in the LG modal plane with random complex coefficients, rotation of the speckle patterns is achieved at specific propagation distances and at a rotation rate given by:

$$\Delta p\ \Delta\psi = \Delta l\beta + 2\pi N \quad (6)$$

$$\dot{\beta} = \frac{d\beta}{dz} = \frac{\Delta l}{\Delta n}\frac{d\psi(z)}{dz} \quad (7)$$

Where β is the rotation angle between two self-imaged planes, N is any integer extending the 2π phase ambiguity, and Δl and Δp are the mode-index differences for the azimuthal and radial indices, respectively.

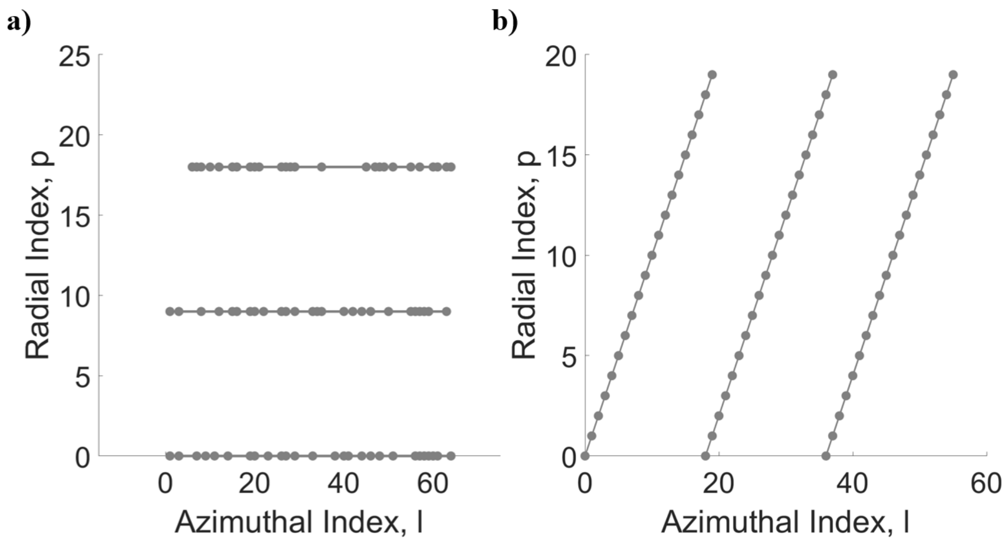

Fig. 2. Laguerre Gaussian modal plane realizations of speckle patterns with propagation order: a) scaled self-imaging (reoccurrences of the scaled speckle pattern at different locations) and b) rotated self-imaging (reoccurrences of the scaled and rotated speckle pattern at various locations). The indicated modes are selected with random complex coefficients.

3. Generation of order-disordered speckles

For SSIS, we generate random complex fields, superimposing LG modes where each line holds the same number of randomly selected modes and different arbitrary coefficients, as seen in Fig. 2. A). We select between 25 and 30 modes per horizontal line, separated by 9 radial indices and a maximum azimuthal index of 70, each with its corresponding complex value. However, one limitation to this approach is the resulting symmetry where the top and bottom areas of the beam are mirrors of themselves (Supplementary 1). Figure 3 shows four different intensity distributions along one Rayleigh range (z_R). Figures b) and d) correspond to z = 0.36, 0.84z_R , being self-images of a), z = 0. Figure c) is an intermediate plane with no significant cross-correlation. Figures e) – h) correspond to the phase profiles from 0 – 2π of the intensity distributions above. See supplementary movies 1 and 2 for simulated intensity and phase profiles while propagating through 0-2z_R, correspondingly.

In the case of ASIS, we select 20 modes per line at a separation of 18 azimuthal indices, with 20 being the maximum value for the radial index, as seen in Fig. 2. b). One would think that a large number of modes would lead to a speckle pattern with a more random appearance. However, this is not always the case, since increasing the radial index significantly with respect to the number of modes can lead to a ring-shaped speckled beam. Furthermore, note that the azimuthal index has a relatively larger value than the radial index; this is due to the need for high-order solutions to break the circular symmetry of LG modes.

Therefore, this modal selection leads to a self-imaging field while generating a rotating disordered beam. Figure 4 shows four different intensity distributions. Figures b) and d) correspond to z = 0.18, $0.36z_R$, being self-images of a), z = 0. Figure c) is an intermediate plane with no significant cross-correlation. Figures e) – h) correspond to the phase profiles from 0 – 2π of the intensity distributions above. For simplification, we define our reference beam waist constant, $w_z = w_0$, allowing for a more rigorous analysis. See supplementary movies 3 and 4 for simulated intensity and phase profiles while propagating through 0-$2z_R$, correspondingly.

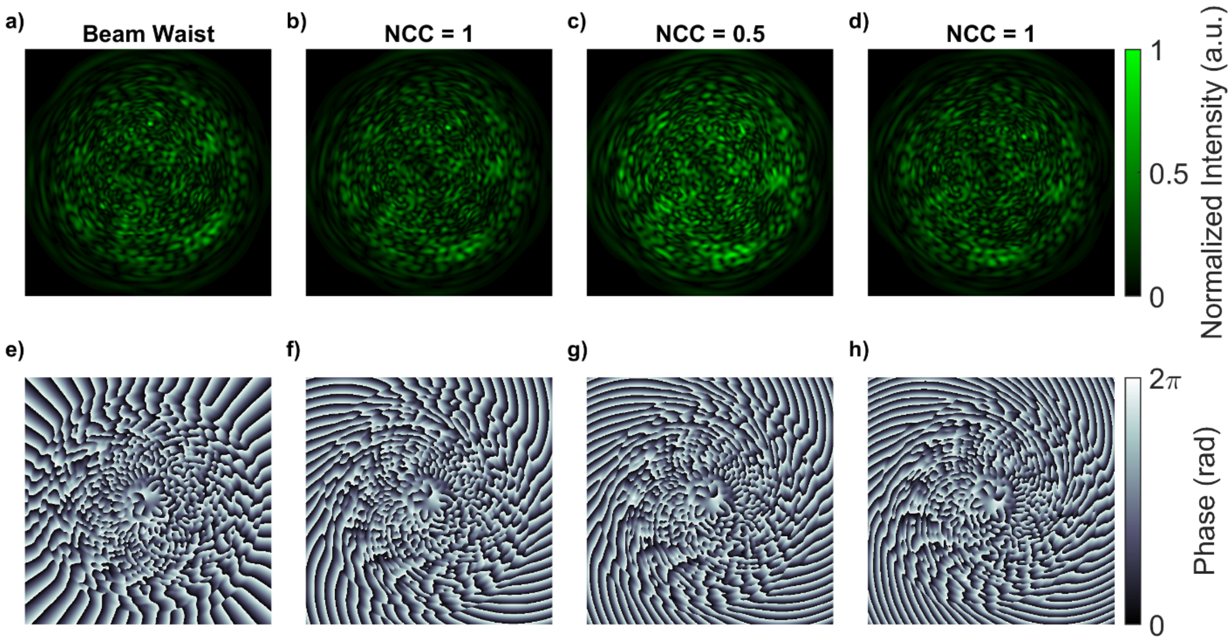

Fig. 3. Realization of a speckle pattern with the scaled self-imaging (SSIS) speckles. a) The (simulated) intensity pattern resulting from an engineered superposition of LG modes at z = 0 b) and d) are the corresponding speckle patterns at z = $0.36z_R$ and 0.84 z_R, where the normalized cross-correlation is 1 (after re-scaling). c) is the speckle pattern corresponding to an uncorrelated intensity distribution at distance z = $0.58z_R$. Figures e) – h) represent the two-dimensional phase profiles corresponding to a) - d). Note: the intensity displays have been saturated for display purposes.

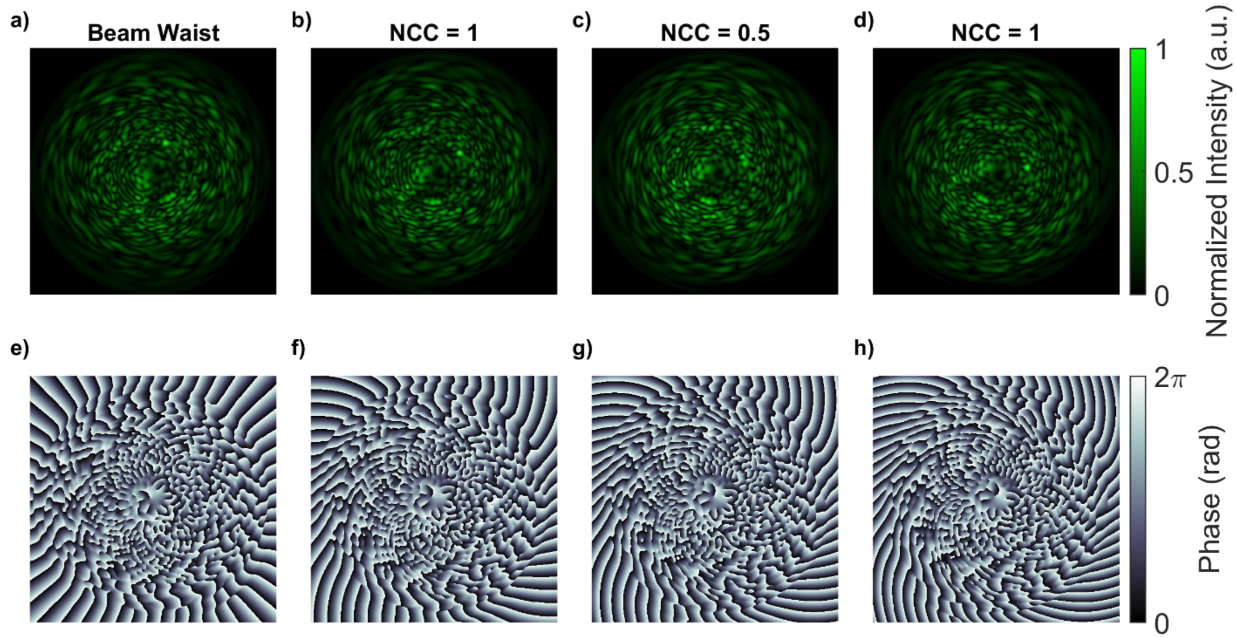

Fig. 4. Realization of a speckle pattern with the controllable rotating scaled self-imaging speckles (ASIS). a) The (simulated) intensity pattern resulting from an engineered superposition of LG modes at z = 0. b) and d) are the corresponding speckle patterns at $z = 0.18z_R$ and $0.36z_R$, where the normalized cross-correlation is 1 (after re-scaling). c) is the speckle pattern corresponding to an uncorrelated intensity distribution at distance $z=0.27z_R$. Figures e) – h) represent the two-dimensional phase profiles corresponding to a) - d). Note: the intensity displays have been saturated for display purposes.

For both cases, the phase presents a random distribution of optical vortices with the addition of a quadratic phase as they propagate. This phenomenon relates to the order-disorder coexistence since the intensity distribution has a random appearance but exhibits an ordered behavior through propagation encoded in the phase. Moreover, we note that optical vortices carry OAM, which can be an interesting characteristic for imaging and sensing applications [43,44].

Furthermore, to understand the behavior of the tailored speckles as they propagate, we calculate the normalized cross-correlation in each example presented above. Figure 5 shows the result for both SSIS and ASIS through propagation along two Rayleigh ranges of the fundamental Gaussian beam. The high cross-correlation indicates the intensity distribution repetition at a distance Δz. SSIS demonstrates its non-periodic repetition three times with quasi-repetition in between self-imaged planes. In the case of ASIS, there is repetition six times, while accounting for a total rotation of 185º. Note that the NCC between two speckle patterns will never be zero due to the large finite number of grains having the same statistical distribution.

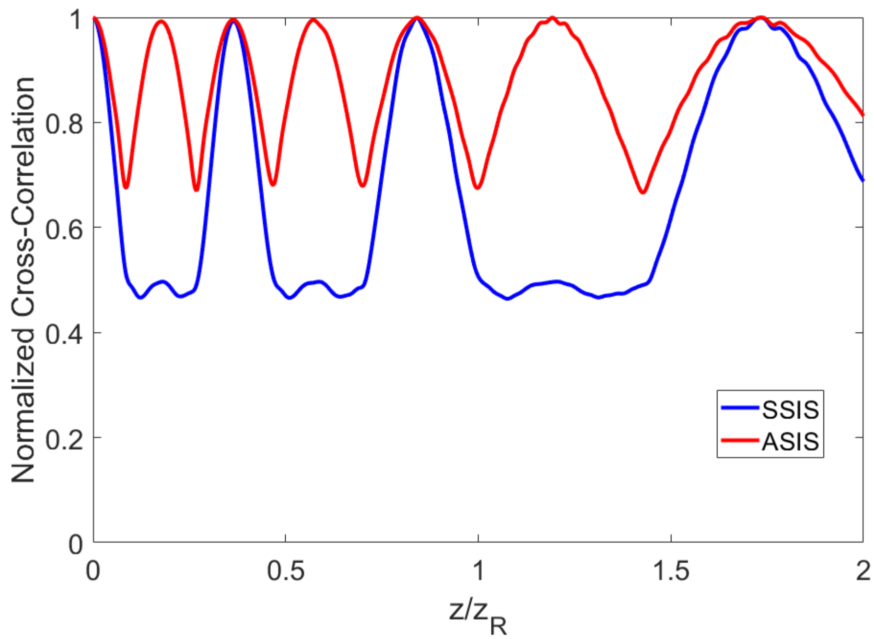

Fig. 5. Normalized cross-correlation for SSIS and ASIS fields along propagation showcasing the non-periodic repetition. (blue) The SSIS patterns of Fig. 3 present three self-images within two Rayleigh ranges as indicated by the cross-correlation peaks. (red) The ASIS patterns of Fig. 4 present six self-images within two Rayleigh ranges. Note: The cross-correlation is calculated after the corresponding azimuthal rotation and re-scaling of the speckle patterns obtained at each transverse plane.

The helical phase profile is a characteristic of beams carrying OAM, commonly represented as $\hbar l$, $\hbar$ being the reduced Planck's constant. Consequently, optical singularities arise at the beam axis where the intensity is null, and the phase is undefined, leading to the appearance of vortices. The phase profile around each of these is increasing monotonically in multiples of 2π. The study of optical vortices propagating in free-space has helped characterize these fields and known superpositions of them [45-48]. OAM beams have been extensively studied for optical tweezers, quantum entanglement, and communications [49-56]. By plotting the OAM singularities of SSIS and ASIS fields through propagation, we can observe the rotational dynamics for both cases, as illustrated in Figure 6. Each plot indicates the rotational properties of the speckle field for both OAM polarities (+1 and -1). Interestingly, most of the rotation occurs in the first Rayleigh range. Furthermore, it should be noted that the azimuthal rotation is not continuous, which is explained by the mode-dependent contributions of the individual OAM components and the fact that the field intensities themselves are not continuously rotating.

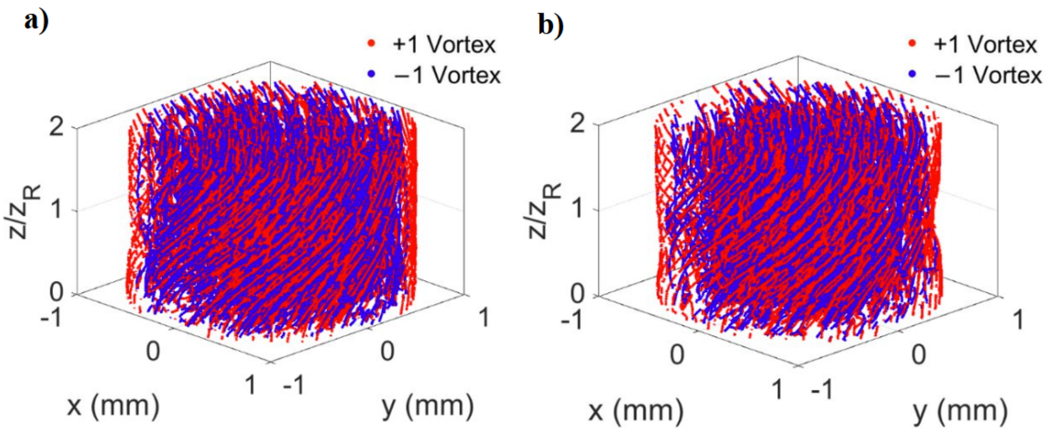

Fig. 6. Optical vortices through 2 Rayleigh ranges of propagation. A) Optical vortices of SSIS through propagation after rescaling, and b) similarly for ASIS.

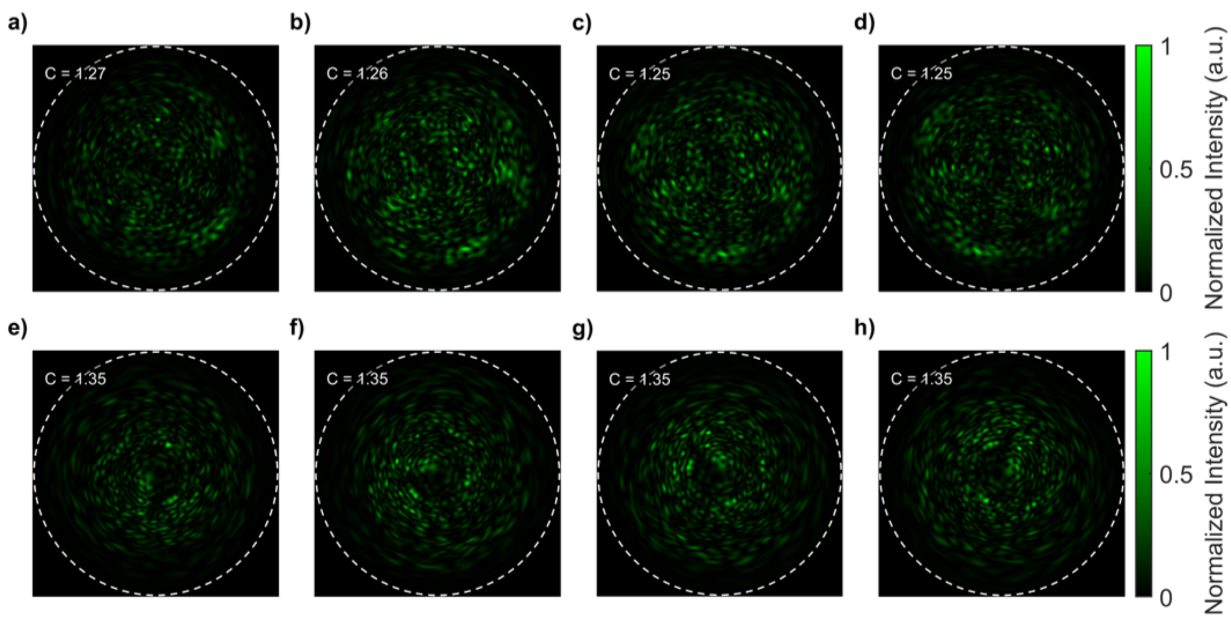

Fig. 7. Contrast analysis of simulated intensity distributions at different planes along two Rayleigh ranges for both modalities. The top row showcases the intensity distribution for SSIS corresponding to z = 0, 0.5, 1, 2 z_R, respectively (a-d). The bottom row corresponds to the case of ASIS from z = 0, 0.5, 1, 2 z_R, respectively (e-h). The contrast, displayed in the left corner of each plane, was calculated inside the ring displayed in a dashed line. These intensity distributions were normalized to their max for visualization purposes.

We perform a contrast analysis for both SSIS and ASIS modalities, defined as

$$C = \frac{\sigma_I}{\langle I \rangle} \tag{8}$$

where I is the speckle intensity distribution, σ_I is the intensity standard deviation, and $\langle I \rangle$ denotes the ensemble average of the intensity [2]. Rayleigh distributions are used to determine the properties of speckles in the strong scattering regime. Fully developed speckles are characterized by $C = 1$. However, by controlling the statistics, non-Rayleigh speckles achieve a higher contrast

[4]. Both cases demonstrate a speckled pattern with higher contrast, with SSIS being $C = 1.26$ and ASIS being $C = 1.35$. This can be seen in figures 7 (a)-(d) and (e)-(h), respectively. The speckle distribution maintains a large number of speckles, which is proportional to the number of optical vortices, while achieving a high contrast. As a result of the high contrast, the PDF will be altered with a longer tail.

To further characterize the random speckle fields, we examine their statistical properties throughout propagation. We calculate the (PDF) for both realization cases above, SSIS and ASIS, as a function of the ratio of intensity over the mean intensity. We compare the PDFs with a negative exponential intensity distribution, which is the typical case of randomly generated speckle patterns, in both linear and logarithmic scales (Figures 8(a) and (b), respectively). The steepness of both PDF functions originated from the high contrast and narrow intensity distribution of the speckle fields, indicating a high concentration of bright and dark spots. This reveals that the strong spatial fluctuations are maintained with minimal intermediate intensity values. This characteristic appears to be constant through propagation.

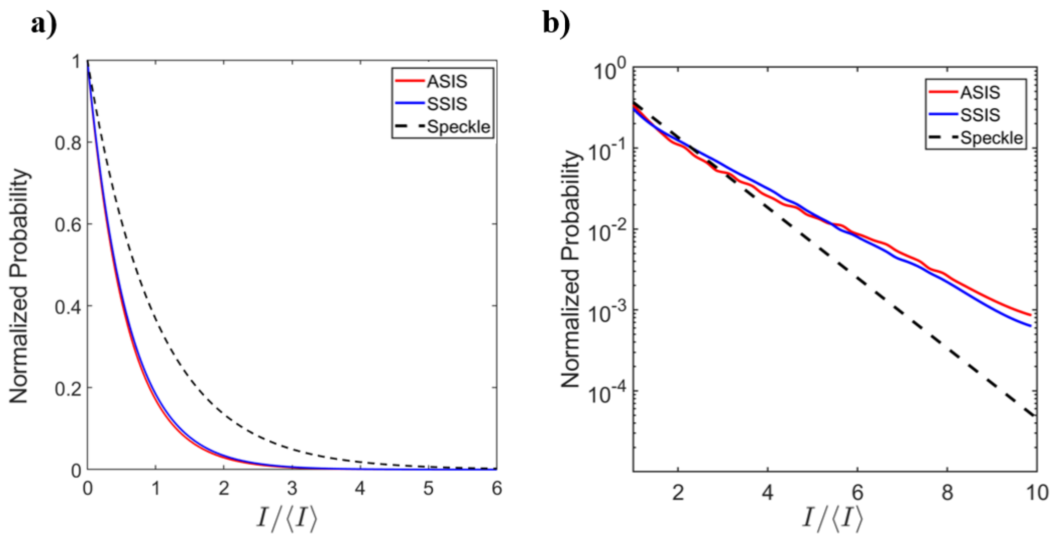

Fig. 8. Probability Density Functions (PDFs) in linear and logarithmic scale for the intensity of random speckle patterns with propagation order: a) linear plot of both modalities' realizations demonstrating a steeper profile than the theoretical decay of randomly generated speckle patterns with a negative exponential profile (Rayleigh statistics), plotted as the dashed line. b) logarithmic plot of the PDFS showcasing the enhanced contrast.

4. Experimental Results

We computationally calculate the complex amplitude $A(\mathrm{x}, \mathrm{y})$ and the phase profile $\varphi(\mathrm{x}, \mathrm{y})$, and encode them into a single phase-only off-axis computer-generated hologram (CGH) on an SLM. We utilize Arrizón's method for both modalities [57]:

$$\alpha\ (x, y) = f(A) \sin(\varphi(x, y) + \theta_c) \tag{9}$$

where $J_1[f(A)] = A$, and θ_c is the carrier frequency chosen to minimize the crosstalk among orders, enhancing a large separation of the first orders concerning the DC term. As a result of utilizing this technique, there is a reduction of the required phase range modulation to $\Delta\varphi \cong 1.17\pi$. Figure 9 shows the two generated CGHs for the SLM, (a) for the SSIS modality and (b) for the ASIS modality.

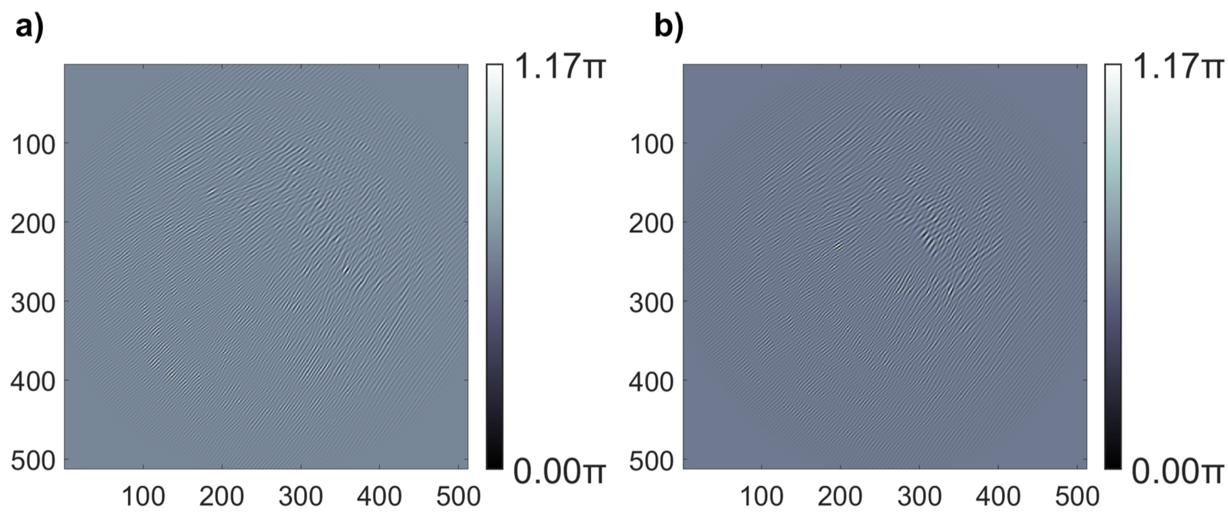

Fig. 9. Phase-only Computer Generated Holograms (CGHs) for a) SSIS, b) ASIS modalities with a phase range modulation to $\Delta\varphi \cong 1.17\pi$.

A continuous wave (CW) laser is vertically polarized and magnified through a telescope to match the size of our 512x512 phase-only SLM, followed by a Fourier lens to capture the desired encoded intensity distribution and wavefront. This is illustrated in figure 10.

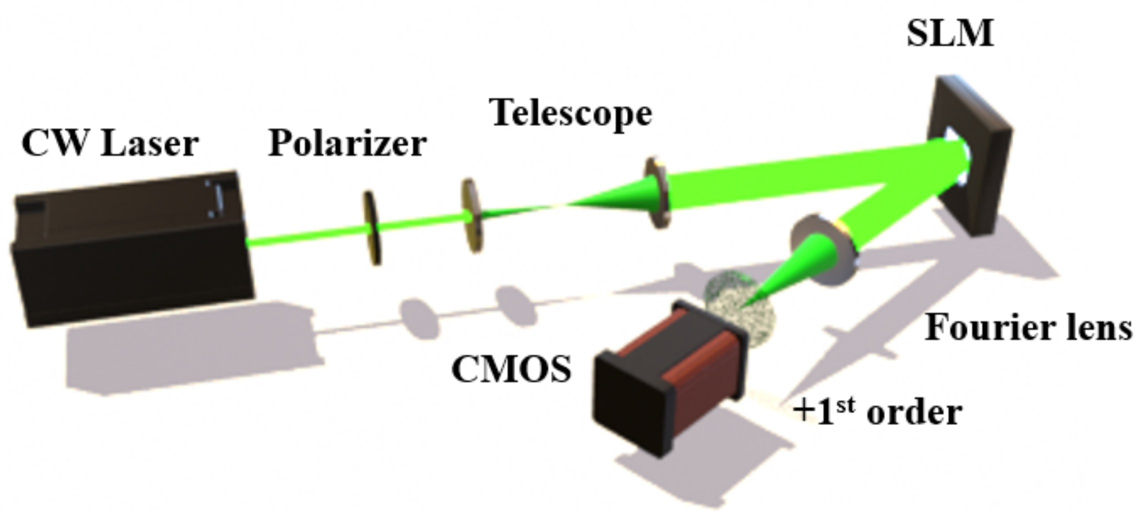

Fig. 10. Experimental setup: a CW laser is vertically polarized, magnified with a telescope to match the SLM dimensions. This has he encoded phase-only hologram, which is Fourier transformed with a lens at the appropriate distances. A CMOS camera records the speckle patterns at different axial locations.

By sliding the camera along the *+z-axis,* we can observe the rotation and intensity repetition of the speckle patterns at the corresponding planes through propagation captured by the CMOS camera. Figure 11, top row, shows the experimental intensity distributions through propagation for the SSIS modality, a) being the beam waist ($z = 0$), b) and d) are the first and second self-imaging planes with NCC=1 after re-scaling, and c) is the speckle pattern corresponding to a not highly correlated intensity distribution. The bottom row (e-h) shows the experimental intensity distributions for the ASIS modality through propagation. e) is the beam waist, f) and h) are the first self-imaging planes, and g) is not a highly correlated distribution. Prior to computing the NCC between the images, the recorded intensities were filtered with a Gaussian kernel. This preprocessing suppresses high-spatial-frequency noise originated from the detector and experimental fluctuations, which is not attributed to propagation-invariance. The filter bandwidth was chosen to not tailor or suppress any spatial frequency associated with the originally formed beam. Note that the images being displayed are slightly saturated for visibility and easier tracking of optical vortices.

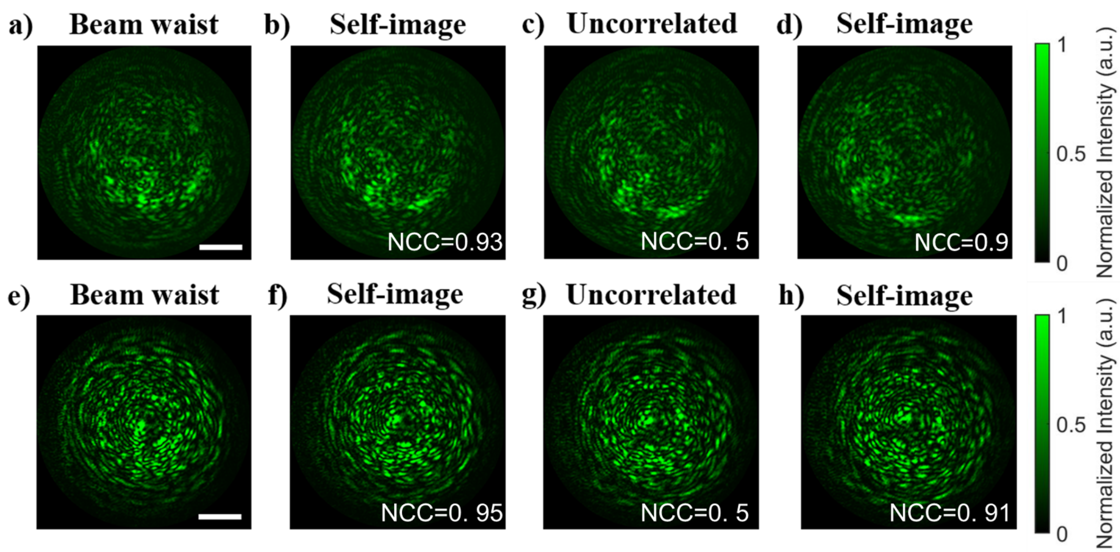

Fig. 11. Experimental demonstration of SSIS and ASIS. The figure shows the azimuthally rotated self-imaged planes with their corresponding normalized cross-correlation (NCC) values through propagation captured by a CMOS camera**.** The top row showcases the experimental intensity distribution for SSIS modality, where a) is the beam waist (Fourier plane), b) and d) are the first and second self-imaging planes, respectively, and c) is a not highly correlated pattern. The bottom row corresponds to the intensity distribution for ASIS modality, with e) being the beam waist, f) and h) are the first and second self-imaging planes, respectively, and g) is a not highly correlated pattern. Scale bar is 0.5 mm.

5. Conclusion

In conclusion, we have demonstrated the design and experimental generation of random speckle patterns with azimuthal propagation order. Via a superposition of LG modes with random complex coefficients, the engineered speckles have deterministic properties such as scaled self-imaging and azimuthal self-imaging through propagation, reflecting an order-disorder coexistence. By generating a phase-only hologram encoding the complex amplitude and desired wavefront, we demonstrated experimentally this phenomenon along the +z-axis. Therefore, one has control over speckle properties while maintaining their random appearance.

The coexistence of order and disorder is attributed to the random superposition of modes, which nevertheless encodes information in the phase of the field, maintaining a precise balance between wavefront vortices and the Gouy phase shift associated with the respective modes.

We emphasize that the class of 3D wave-fields presenting speckle patterns with propagation order is infinite and can be defined by specific characteristics in the modal plane (LG plane in this case). The two realizations presented here demonstrate some of the key characteristics of these wave-fields, while specific constrained optimization can be performed to achieve additional statistical qualities.

The demonstrated control over the propagation dynamics of speckles opens avenues for applications where both deterministic and random behaviors are desired. Different examples include dynamic speckle illumination, super-resolution imaging, and optical manipulation, where coherence and correlation properties can impact the performance.

The data that support the findings of this study are available from the corresponding author upon reasonable request.

We thankfully acknowledge support through NSF grant 1548924, Science and Technology Center on Real-Time Functional Imaging (STROBE), and NIH grant 1R21EY037083-01.

References

1. J. W. Goodman, "Some fundamental properties of speckle*," J. Opt. Soc. Am. 66, 1145-1150 (1976)
2. J. W. Goodman, *Speckle Phenomena in Optics: Theory and Applications* (Roberts and Company Publishers, 2007).
3. J. P. Amaral, E. J. S. Fonseca, and A. J. Jesus-Silva, “Tailoring speckles with Weibull intensity statistics,” Phys. Rev. A 92, 063851 (2015).
4. Y. Bromberg and H. Cao, “Generating non-Rayleigh speckles with tailored intensity statistics,” Phys. Rev. Lett. 112, 213904 (2014).
5. N. Bender, H. Yılmaz, Y. Bromberg, and H. Cao, “Customizing speckle intensity statistics,” Optica 5, 595 (2018).
6. N. Bender, H. Yılmaz, Y. Bromberg, and H. Cao, “Creating and controlling complex light,” APL Photonics 4, 110806 (2019).
7. L. Devaud, B. Rauer, J. Melchard, M. Kühmayer, S. Rotter, and S. Gigan, “Speckle Engineering Through Singular Value Decomposition of the Transmission Matrix,” Phys. Rev. Lett. 127, 093903 (2021).
8. R. Liu, B. Qing, S. Zhao, P. Zhang, H. Gao, S. Chen, and F. Li, Generation of Non-Rayleigh Nondiffracting Speckles, Phys. Rev. Lett. 127, 180601 (2021).
9. Z. Ye, W. Hou, J. Zhao, and J. Xiong, “Vortex speckles with customized symmetry and spatial correlations,” Phys. Rev. Appl. 18(6), 064060 (2022)
10. Nicholas Bender, Henry Haig, Demetrios N. Christodoulides, and Frank W. Wise, "Spectral speckle customization," Optica 10, 1260-1268 (2023)
11. S. Han, N. Bender, and H. Cao, “Tailoring 3D speckle statistics,” Phys. Rev. Lett. 130, 093802 (2023).
12. R. Piestun and J. Shamir, “Control of wave-front propagation with diffractive elements”, *Opt. Lett.* 19, 771-773 (1994)
13. R. Piestun, B. Spektor, J. Shamir, “Wave fields in three dimensions: Analysis and synthesis” J. *Opt. Soc. Am. A* 13, 1837-1848, (1996).
14. R. Piestun and J. Shamir, “Synthesis of 3D light fields and applications”, *Proceedings of the IEEE* , 90, 222 –244 (2002)
15. D. M. Cottrell, J. M. Craven, and J. A. Davis, "Nondiffracting random intensity patterns," Opt. Lett. 32, 298-300 (2007)
16. M. Boguslawski, S. Brake, J. Armijo, F. Diebel, P. Rose, and C. Denz, "Analysis of transverse Anderson localization in refractive index structures with customized random potential," Opt. Express 21, 31713-31724 (2013)
17. I. Cázares-Aguilar, J.C. Atenco, P. Martínez-Vara, F. Cubillos-Morales, I. Julián-Macías, G. Martínez-Niconoff, “Stochastic modulation of the Montgomery rings to generate the self-imaging effect with revival features”, Results in Optics, 16, 100714 (2024)
18. C. Ventalon and J. Mertz, Quasi-confocal fluorescence sectioning with dynamic speckle illumination, Opt. Lett. 30, 3350 (2005).
19. C. Ventalon and J. Mertz, “Dynamic speckle illumination microscopy with translated versus randomized speckle patterns,” Opt. Express 14, 7198–7209 (2006).
20. E. Mudry, K. Belkebir, and A. Girard et al., “Structured illumination microscopy using unknown speckle patterns,” Nat. Photonics 6(5), 312–315 (2012).

21. Hasan Yilmaz, Elbert G. van Putten, Jacopo Bertolotti, Ad Lagendijk, Willem L. Vos, and Allard P. Mosk, "Speckle correlation resolution enhancement of wide-field fluorescence imaging," Optica 2, 424-429 (2015)
22. T. Chaigne, J. Gateau, M. Allain, O. Katz, S. Gigan, A. Sentenac, and E. Bossy, "Super-resolution photoacoustic fluctuation imaging with multiple speckle illumination," Optica 3, 54–57 (2016).
23. T. Chaigne, J. Gateau, M. Allain, O. Katz, S. Gigan, A. Sentenac, and E. Bossy, Super-resolution photoacoustic fluctuation imaging with multiple speckle illumination, Optica 3, 54 (2016).
24. J. Idier, S. Labouesse, M. Allain, P. Liu, S. Bourguignon, and A. Sentenac, On the superresolution capacity of imagers using unknown speckle illuminations, IEEE Trans. Comput. Imaging 4, 87 (2018)
25. A. Caravaca-Aguirre, S. Singh, S. Labouesse, M. V. Baratta, R. Piestun, and E. Bossy, "Hybrid photoacoustic-fluorescence microendoscopy through a multimode fiber using speckle illumination," *APL Photonics* 4, 096103 (2019)
26. G. Giroussens, S. Labouesse, M. Allain, T. Mangeat, A. Sentenac, and J. Idier, "Fast super-resolved reconstructions in fluorescence random illumination microscopy (RIM)", Tech. Rep. https://hal.science/hal-04139086 (2023).
27. Evolene Premillieu, Antonio M. Caravaca-Aguirre, Simon Labouesse, Kristina Irsch, and Rafael Piestun, "Aberration correction in epi-fluorescence microscopy using unknown speckle illumination," Opt. Express 32, 37658-37667 (2024)
28. P. R. Rodriguez, B. Hwang, K. Irsch, and R. Piestun, "Enhanced 3D Resolution via Boosted Speckle Illumination and Point Spread Function Estimation," in *Optica Imaging Congress 2025 (3D, DH, COSI, IS, pcAOP,RadIT)*, Technical Digest Series (Optica Publishing Group, 2025), paper ITh1D.2.
29. K. Dholakia and T. Cižmár, "Shaping the future of manipulation," ˇ Nat. Photonics 5, 335–342 (2011).
30. G. Volpe, L. Kurz, A. Callegari, G. Volpe, and S. Gigan, Speckle optical tweezers: Micromanipulation with random light fields, Opt. Express 22, 18159 (2014).
31. S. Gigan, et al., "Roadmap on wavefront shaping and deep imaging in complex media," J. Phys. Photon. 4, 042501 (2022).
32. J. H. Shapiro, "Computational ghost imaging", Phys. Rev. A **78**, 061802 (2008).
33. O. Katz, Y. Bromberg, Y. Silberberg, Compressive ghost imaging. *Appl. Phys. Lett.* 28 September 2009; 95 (13)
34. D. B. Phillips, Ruiqing He, Qian Chen, G. M. Gibson, and M. J. Padgett, "Non-diffractive computational ghost imaging," Opt. Express 24, 14172-14182 (2016)
35. C. Bechinger, R. Di Leonardo, H. Löwen, C. Reichhardt, G. Volpe, and G. Volpe, "Active particles in complex and crowded environments," Rev. Mod. Phys. 88, 045006 (2016).
36. E. Pinçe, S. K. Velu, A. Callegari, P. Elahi, S. Gigan, G. Volpe, and G. Volpe, "Disorder-mediated crowd control in an active matter system," Nat. Commun. 7, 10907 (2016)
37. R. Piestun, Y. Y. Schechner, J. Shamir, "Self-imaging with finite energy", *Opt. Lett.* 22, 200-202 (1997)
38. Rafael Piestun, Yoav Y. Schechner, and Joseph Shamir, "Propagation-invariant wave fields with finite energy," J. Opt. Soc. Am. A 17, 294-303 (2000)
39. Rafael Piestun and Joseph Shamir, "Generalized propagation-invariant wave fields," J. Opt. Soc. Am. A 15, 3039-3044 (1998)

40. A. Y. Bekshaev, M. S. Soskin, and M. V. Vasnetsov, “Angular momentum of a rotating light beam,” Opt. Comm. 249, 367-378 (2005)
41. H. F. Talbot, “Facts relating to optical science,” Philos. Mag. 9, 401–407 (1836).
42. W. Duane Montgomery, "Self-Imaging Objects of Infinite Aperture*," J. Opt. Soc. Am. 57, 772-778 (1967)
43. Severin Fürhapter, Alexander Jesacher, Stefan Bernet, and Monika Ritsch-Marte, "Spiral phase contrast imaging in microscopy," Opt. Express 13, 689-694 (2005)
44. J. Zeng, Y. Dong, Y. Wang, J. Zhang and J. Wang, "Optical Imaging Using Orbital Angular Momentum: Interferometry, Holography and Microscopy," *Journal of Lightwave Technology*, 41,7, 2025-2040, (2023)
45. G. Indebetouw, Optical Vortices and Their Propagation. *Journal of Modern Optics*, *40*(1), 73–87 (1993).
46. M. S. Soskin, V. N. Gorshkov, M. V. Vasnetsov, J. T. Malos, and N. R. Heckenberg, “Topological charge and angular momentum of light beams carrying optical vortices,” Phys. Rev. A 56, 4064–4075 (1997).
47. M. J. Padgett and L. Allen, "The Poynting vector in Laguerre–Gaussian laser modes," Opt. Commun. 121, 36–40 (1995)
48. A. Bekshaev, K. Y. Bliokh, and M. Soskin, “Internal flows and energy circulation in light beams,” J. Opt. 13, 053001 (2011).
49. Padgett, M., Bowman, R. Tweezers with a twist. *Nature Photon* **5**, 343–348 (2011).
50. Wang, J., Yang, JY., Fazal, I. *et al.* Terabit free-space data transmission employing orbital angular momentum multiplexing. *Nature Photon* **6**, 488–496 (2012).
51. Willner AE, Wang J, Huang H. Applied physics. A different angle on light communications. Science. 337,655-656 (2012)
52. Jing Du and Jian Wang, High-dimensional structured light coding/decoding for free-space optical communications free of obstructions, Opt. Lett. 40, 4827-4830 (2015)
53. Zhang, Y., Agnew, M., Roger, T. *et al.* Simultaneous entanglement swapping of multiple orbital angular momentum states of light. *Nat Commun* **8**, 632 (2017).
54. Alan E. Willner, Yongxiong Ren, Guodong Xie, Yan Yan, Long Li, Zhe Zhao, Jian Wang, Moshe Tur, Andreas F. Molisch, Solyman Ashrafi; Recent advances in high-capacity free-space optical and radio-frequency communications using orbital angular momentum multiplexing. *Philos Trans A Math Phys Eng Sci* 28 (2017)
55. R. Chen, H. Zhou, M. Moretti, X. Wang and J. Li, "Orbital Angular Momentum Waves: Generation, Detection, and Emerging Applications," in *IEEE Communications Surveys & Tutorials*, vol. 22, no. 2, pp. 840-868 (2020)
56. Wang, Qian-Ke and Wang, Fang-Xiang and Liu, Jun and Chen, Wei and Han, Zheng-Fu and Forbes, Andrew and Wang, Jian, “High-Dimensional Quantum Cryptography with Hybrid Orbital-Angular-Momentum States through 25 km of Ring-Core Fiber: A Proof-of-Concept Demonstration,” Phys. Rev. Appl., 15,6, 064034 (2021)
57. Victor Arrizón, Ulises Ruiz, Rosibel Carrada, and Luis A. González, "Pixelated phase computer holograms for the accurate encoding of scalar complex fields," J. Opt. Soc. Am. A 24, 3500-3507 (2007)